A new capacitive inductive system design for LASER-induced kilotesla magnetic field generation

Ahmet Nuri Akay * (iD)
TOBB University of Economics and Technology, Engineering Department, Ankara, Türkiye, anakay.tobbetu@gmail.com
Melda Varol (iD)
TOBB University of Economics and Technology, Engineering Department, Ankara, Türkiye, melda.varol@hotmail.com
Erol Kurt (iD)
Gazi University, Technology Faculty, Department of Electrical and Electronics Engineering, Ankara, Türkiye, ekurt@gazi.edu.tr

Abstract: This research focuses on exploring the nanosecond laser-driven coil systems capable of generating kT magnetic fields and the diverse applications of this system. Through investigating the effects of laser parameters and coil structures, the aim of this study is to unveil the physics of these generated intense magnetic fields. The outcomes gained from this research give an important and fundamental understanding on high magnetic field production, informing the development in laser-driven systems. The implications of this study extend to plasma physics, astrophysics simulations and fusion research. Furthermore, the study explains the advantages and applications of these intense magnetic fields and includes measurements of laser pulse powers according to coil materials.

Cite this paper as:	Akay, A.N., Varol, M., & Kurt, E. A new capacitive inductive system design for LASER-induced kilotesla magnetic field generation. *Journal of Energy Systems 2024; 8*(1): 75-88, DOI: 10.30521/jes.1439709

1. INTRODUCTION

For researches in high energy density science (HED) [1], astrophysics, materials science, atomic and nuclear physics [2,3] and nuclear fusion reactions; capability of generating, localizing and controlling strong magnetic fields have great importance. Material properties vary in all aspects (atoms, molecules, plasmas) when they are under the influence of strong magnetic fields (i.e. *B*) [4,5,6,7]. For example, at this point we can mention about astrophysical plasmas having the temperature and density values of $10 < T < 100$ eV and $10^{17} < n < 10^{19}$ cm^{-3}, respectively may be magnetized with approximately 10 T magnitude of magnetic fields [8,9,10,11,12]. The development of quasi-static magnetic fields connected with laser facilities has been achieved through the implementation of capacitor pulsed discharges within solenoidal structure, known as magnetic pulsers [13,14,15,16,17,18,19,20]. Nonetheless, specific physical constraints restrict the maximum achievable fields at approximately 40 T which is typically reduced to a safer operational level of around 20 T [21,22]. In recent researches involving intense laser-plasma interactions at limited spatial and temporal dimensions, measurements have unveiled the occurrence of magnetic field generation, reaching several kilotesla [13,14,15,16,]. Alternatively, by Daido et al, the interaction of capacitor-coil targets and powerful lasers was proposed in 1980s [23]. An example schematic diagram of a laser-driven capacitor - coil type target is shown in Fig. 1. These target type offers the advantage of being relatively low cost when produced in large amounts. They also are adaptable, accommodating laser structures with high repetition rates. Notably, these coils form an open geometrical shape, ensuring convenient access for various diagnostic perspectives. They also enable the magnetization of secondary specimens, potentially driven by a secondary laser beams or other induced particle beams.
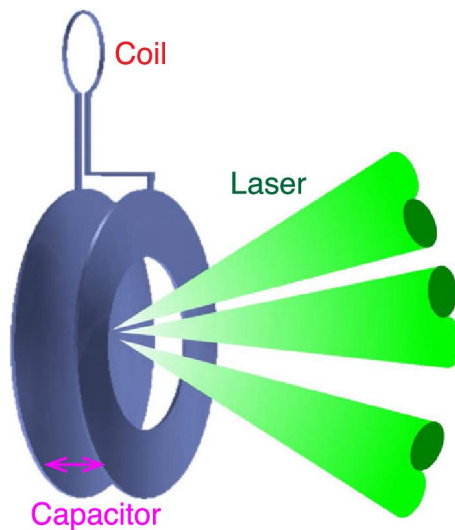

Figure 1. Schematic representation of a sample laser-driven structure, namely, capacitor coil.

It has been established that employing a long pulse with a nanosecond-class, high energy amount of several hundreds of joules to a small coil target can yield a quasi-static magnetic field exceeding 1 kT over a duration of one nanosecond [15,16,17]. For instance, a magnetic field reaching up to 4 kT was successfully produced by compressing a 6-T seed magnetic field at the OMEGA laser facility and this played a crucial role as it was used in conducting a inertial fusion experiment in USA [18]. The magnitude of the magnetic field differs under various conditions and depended on laser intensity [1,24], laser frequency [25], and pulse duration [26,27]. Fujioka et al [1] have further advanced this concept, successfully reaching approximate magnetic field strength of 1.5 kT at a distance of 0.65 mm from the U-turn coil which was powered by a 1 kJ laser pulse and attained an unmatched quasi static *B*-field amplitude. Recently, Morita et al. [28] obtained the topological structure of the magnetic field using a longer pulse (10 nanoseconds), high power (0.5 TW) laser with an U-shaped metal target. An example

modelization of a laser-driven capacitor-coil target is shown in Fig. 1. On the contrary, Zhu et al., suggested using only one single open-ended coil, presenting a simpler design [28]. Various coil types are shown in Fig. 2.
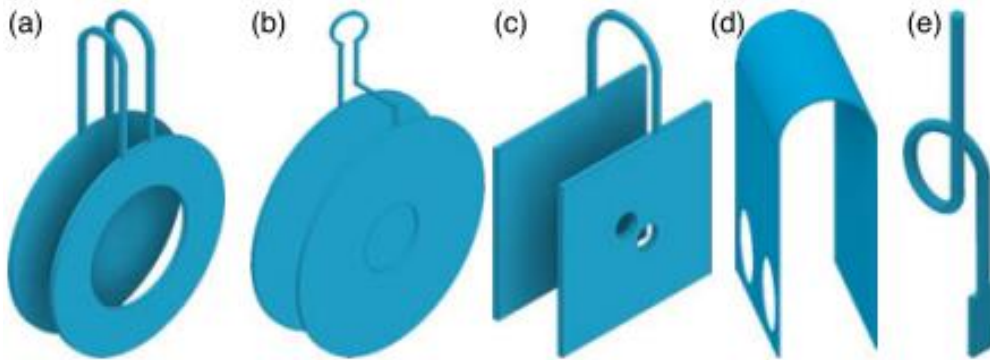

Figure 2. Various Coil Types: (a) Ref. [29], (b) Ref. [15], (c) Ref. [30], (d) Ref. [25], (e) Ref. [28].
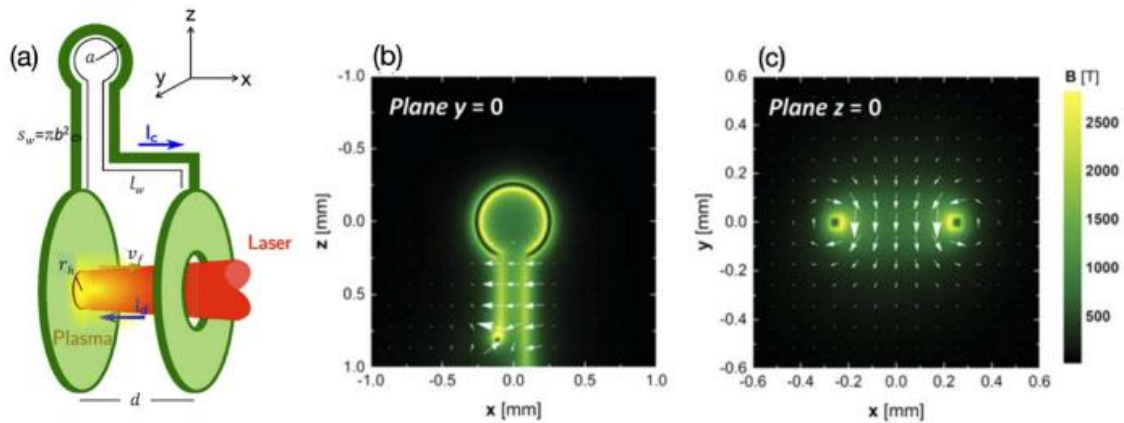

Figure 3. (a) Laser-driven coil which may produce 100-1000 T of a magnetic field [31], the spatial distribution of the magnetic field on (b) x-z plane, (c) x-y plane calculated by RADIA code [15].

A laser-driven coil simply composed by two plates with a single or double wire connection [1,15]. In Figs. 3(b) and (c), the spatial distribution of the magnetic fields on *x-z* and *x-y* planes, respectively are illustrated. These computations were conducted using RADIA code, capable of determining a static magnetic field based on specified current sources [32]. It is noteworthy that for the majority of cases, the indicative magnetic field value corresponds to the center of the coil (located at the origin (0,0,0) in Figs. 3(b,c)) [33]. As well as RADIA, other simulations such as COMSOL, OPERA3D and Ansys Maxwell is able to calculate the dynamics of the magnetic field, deformation caused by Lorentz force etc [34].

Simultaneously, the significance of high-intensity laser systems in generating strong magnetic fields through the induction of powerful electric currents has increased. The development of the Chirped Pulse Amplification (CPA) enabled the laser pulse amplification to achieve an ultra-high energy density [35], which allowed the success in generating extremely strong currents, thereby strong magnetic fields. As a high-intensity laser and plasma interact, the generated magnetic field may have a magnitude as an oscillating laser magnetic field which the generation of hot electrons are affected by [36]. To diagnose this magnetic fields, there commonly magnetic fields diagnostic methods are used in laser-driven capacitor-coil target experiments: *B*-dot method (also known as pick-up coil), optical probe method (Faraday rotation) and proton radiography (deflectometry) method [33,34].

Recently, Peebles et al [37] conducted comprehensive experiments to evaluate the capability of laser-driven coils in generating magnetic field by using various diagnostic methods mentioned above. As a conclusion, it has been found that the laser driven coils do not perform as claimed, failed to produce quasi-static kilotesla-level magnetic fields and are not applicable for the majority of current experiments where it is beneficial to have a field. Notably, their results do not deny the previous experiments including this subject.

In this study, the physics behind generation of magnetic field with laser-driven capacitor coils, necessary measurements and essential formulas for calculations will be presented and briefly explained. Additionally, a new design for an inductive capacitive system will be showcased and the observed dynamics of the generated magnetic field from the new design will be highlighted.

2. LASER-INDUCED MAGNETIC FIELD GENERATION

Recent studies have led to the development of several methods to generate a strong magnetic field exceeding 100 T at laser facilities with high intensity and power, all accomplished without the necessity for compression. Despite the researches that has been done in this field, this generation mechanism has not yet been understood well due to lack of experimental data. As shown in Fig. 4; kilojoule-scale, nanosecond laser pulses are directed to the first disk through the hole in the second disk. The increased heat from laser pulse power overcomes the Coulomb barrier between the electrons, creating a plasma between disks. Following the electron density gradient, the hot electrons encounter with the second disk by moving through the plasma which leads to first disk to charge positive and the second disk to charge negative. The difference in voltage between the plates results in an oscillating voltage, causing variable currents circulating between the plates.
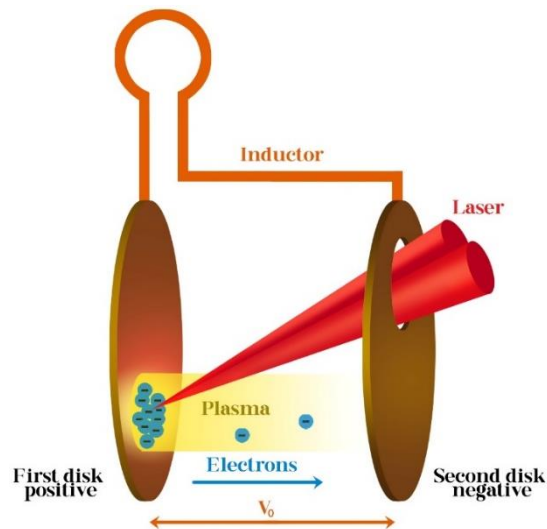

Figure 4. A schematic diagram of a laser-driven coil target

Simultaneously, a magnetic field generation occurs in the space between the plates. The induced current in the system leads to the generation of an additional magnetic field in the inductor. Through vectorial addition, the combined magnitude of the produced magnetic field extends to kilotesla. Alterating material composition of the disk, laser frequency and laser power may contribute to variability in the magnitude of the generated magnetic field, potentially reaching several kilotesla.

Initiated by the laser pulse energy and heat, the process induces plasma formation. The high-speed movement of electrons in the plasma, resembling a current-carrying wire or "conductor", results in the generation of a magnetic field, transforming the disks into a voltage source. Simultaneously, the inductor

produces its magnetic field, further trapping and increasing the density of the plasma, elevating the overall magnetic field's magnitude. The cumulative effect leads to the achievement of a kilotesla-level magnetic field. The continuous nature of this process enables the application of the provided equations in ongoing calculations.

3. FORMULATION OF LASER-INDUCED MAGNETIC FIELD GENERATION

The electromotive force (ie. ε) is the maximum possible voltage that the system can provide between its terminals and for the system described in Fig. 4, it is the potential difference between the two disks. This system initially exhibits the characteristics of an "RL Circuit" followed by a transition to an "RLC Circuit", however, the magnitude of "R" is negligible. Therefore, equations for an "LC Circuit" may be used.

The inclusion of the coil in the system with self-inductance prevents sudden fluctuations in the circuit current, leading the system to behave as an RL Circuit. The inductor produces a back emf, opposing immediate shift in the circuit's current and attempts to maintain the current at its prior level. Kirchoff's law can be applied to an RL Circuit as Eq. (1).

$$\varepsilon(t) - IR - L\frac{dI}{dt} = 0 \qquad (1)$$

IR represents the voltage drop across the resistor. As the equation is derived with the variable change as $x = \left(\varepsilon/R\right) - I$ and $I=0$ at t=0, Eq. (2) is achieved.

$$I = \frac{\varepsilon}{R}\left(1 - e^{-t/\tau}\right) \qquad (2)$$

Eq-(2.2) illustrates the impact of the inductor on the current. τ is the time constant of the circuit as $\tau = L/R$. Time interval is the time required for the current to reach 63.2% of its final value ε/R. With accepting $I_0 = \varepsilon/R$ (the current at the instant), Eq. 2 can be written as Eqs. (2,3).

$$I = I_0\left(1 - e^{-t/\tau}\right) \qquad (3)$$

Due to the induced emf in an inductor, preventing the establishment of current, the battery (voltage generated between the disks) needs to supply more energy compared to a circuit without an inductor. A part of the energy provided converts into internal energy within the resistor, while the remaining energy is stored in the magnetic field of the inductor. With derivations, the energy stored in the magnetic field can be demonstrated as Eq. (4).

$$\frac{dU}{dt} = LI\frac{dI}{dt} \qquad (4)$$

In Eq-(2.4), U represents the energy stored in the inductor at any time. Thus, Eq. (4) gives the deviation of the induced energy in the system.

The system behaves with the characteristic of an LC Circuit afterwards. Due to the initial charge of the capacitor, oscillations in the current occur, alternating between positive and negative values in the circuit. Following the discharge of the capacitor, there is a reduction in the energy stored within the electric field. This discharge process signifies a flow of the current in the circuit, leading to the storage

of the energy within the magnetic field of the inductor. Consequently, an energy transfer occurs from the capacitor's electric field to the inductor's magnetic field. In an LC Circuit, the oscillations eventually result in the occurrence of resonance. For an LC Circuit, the charge of capacitor as a function of time can be written as Eq. (5).

$$Q = Q_{max} \, cos(\omega t + \varphi) \qquad (5)$$

In Eq. (5); Q represents the charge of the capacitor and Q_{max} is the maximum charge of the capacitor where ω is the angular frequency and φ is the phase constant. The formulation for angular frequency (ω) is shown as Eq. (6).

$$\omega = \frac{1}{\sqrt{LC}} \qquad (6)$$

Since Q varies sinusoidally, the current also varies sinusoidally as a function of time and it can be demonstrated as Eq. (7).

$$I = \frac{dQ}{dt} = -\omega \, Q_{max} \, sin(\omega t + \varphi) \qquad (7)$$

The energy of the LC Circuit continuously alternates between the energy stored in the electric field of the capacitor and the energy stored in the magnetic field of the inductor. When the energy peaks in the capacitor, the stored energy in the inductor drops to zero, and inversely, this remains accurate.

4. INDUCTIVE CAPACITIVE LASER INDUCED MAGNETIC GENERATOR

This section showcases our proposed design, referred to simply as "ICLIMG", featuring its individual components. The design includes a coil, a capacitor and a tungsten pin. Tungsten is chosen for the pin since it is an endurable material for high temperatures and an effective conductor to sustain electrons per laser shot. Even with a special screw, one can easily change it with a new one after long laser shots, experimentally.
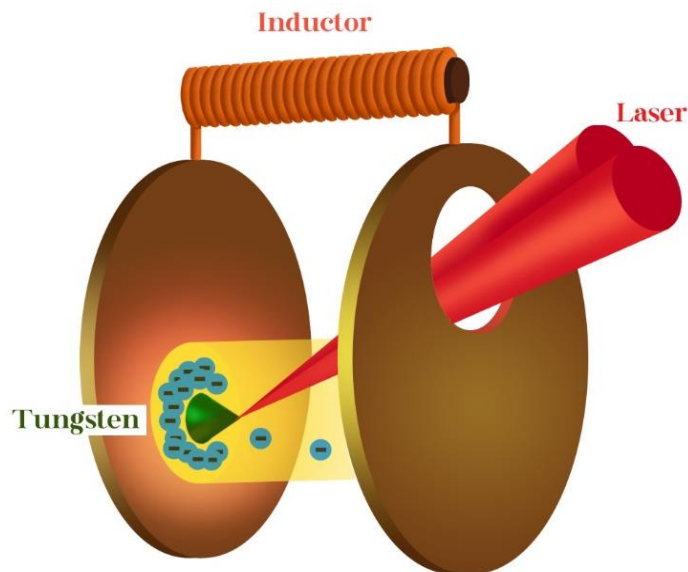

Figure 5. The sketch of the proposed inductive capacitive laser induced magnetic generator (ICLIMG).

In order to minimize the impedance of the capacitive element of the system, we introduce an N-turn coil. This coil would provide the desired inductive reactance (X_L) in order to compensate the capacitive reactance (X_C) arising from the capacitive effect after the interaction with the laser beam. As it is known already, the maximal current flowing from the electrical circuitry of the system is obtained when the impedance becomes minimum. Thus, assigning a clearly defined inductive element is essential to minimize impedance. This is crucial for maximizing the current between the electrical plates.

As the laser pulses interact with the disks, electrons gain kinetic energy, leading to an increase in their speed. This initiates the transfer of electrons towards the other disk, while the remaining protons become more concentrated as they are impacted by the laser pulses. The increased temperature and density enable the protons to surpass the Coulomb barrier, resulting in plasma formation. The combined effect of this magnetic field and the one produced by the voltage exceeds the kilotesla range.

This part of the study explains the material choice for the proposed design, comparing Nickel (Ni) and Tungsten (W) material properties as presented in Table 1. An illustrative laser pulse model was utilized with COMSOL Multiphysics software, features given in Table 2, applying the laser pulses on a two-dimensional plate from the center of the circular domain to simplify the procedure and demonstrate the rationale for the material choice, visualized in Figs. 6 and 7. The results of plasma analysis for Ni are given in Figs. 8-10 and for W are given in Figs. 11-13. Nickel was selected since it was the commonly used material for capacitor coils in the literature. A maximum of 1656.3 K was reached for Ni while 2451.1 K was achieved for W in the first simulation. The comparison of electric potential graph between Ni and W plates is showcased in Fig. 14.

Following the initial simulation, another one was performed to achieve even greater temperatures for the W plate. Nonetheless, a comparison could not be made as it resulted in the melting of Ni. The characteristics of the laser pulse for second simulation are presented in Table 3 and the results are shown with Figs. 15 and 16. A maximum of 3530.1 K was reached according to our finite element analysis simulations.

Table 1. Material Properties of Ni and W [38].

	Nickel (Ni)	Tungsten (W)
Density	8.88 $\left[\frac{g}{cm^3}\right]$	19.3 $\left[\frac{g}{cm^3}\right]$
Atomic Number	28	74
Electronegativity	1.91	1.7
Heat of Fusion	305.6 $[J/g]$	184.2 $[J/g]$
Heat of Vaporization	5862 $[J/g]$	-
Specific Heat Capacity	0.460 $\left[J/_{g.°C}\right]$	0.134 $\left[J/_{g.°C}\right]$
Thermal Conductivity	60.7 $\left[W/_{m.K}\right]$	163.3 $\left[W/_{m.K}\right]$
Melting Point	1728 $[K]$	3643 $[K]$
Boiling Point	2913 $[°C]$	5900 $[°C]$
Emissivity (200-400 °C) (1000 °C)	0.08 0.19	0.15 -

Table 2. The features of the laser pulse used in the simulations for the Ni and W plates.

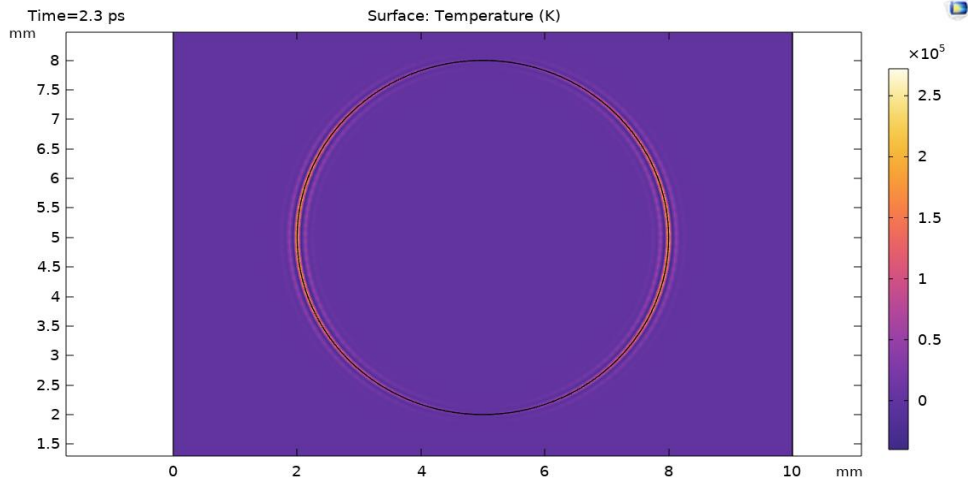| Power of The Laser	$1x10^{15}$ $[W]$
Range	2.3 $[ps]$

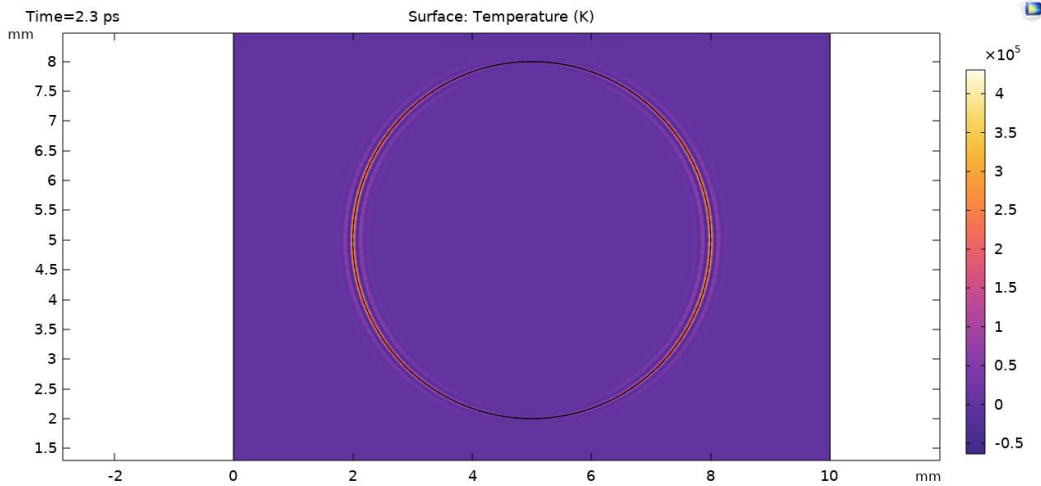*Figure 6. Illustrated laser pulse simulation with using a 2D Plate for Ni.*

Figure 7. Illustrated laser pulse simulation with using a 2D Plate for W.

Examining Figs. 6 and 7, it is indicated that under the same conditions specified in Table 2, Tungsten has the capacity to achieve higher temperatures compared to Nickel. This is attributed to its lower heat capacity, which is notably less than half that of Ni, and significantly higher thermal conductivity. Therefore, we believe that W can be a good material for the laser-induced capacitive inductive system.
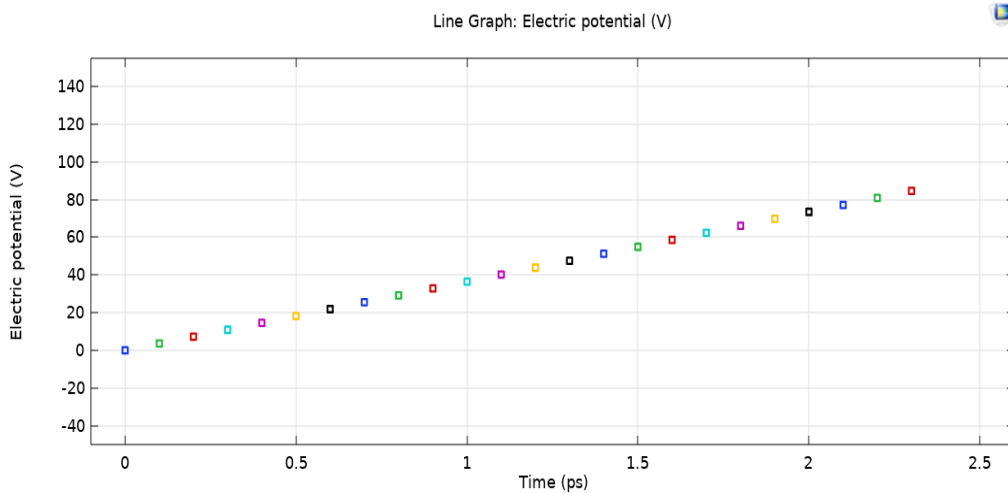

Figure 8. The plot of electric potential versus time in the case of Ni from simulations.
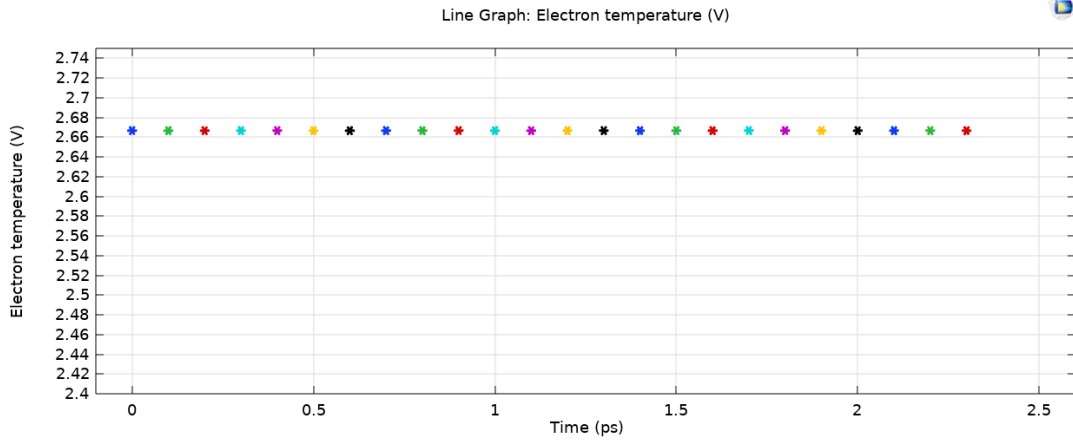
Figure 9. The plot of electron temperature (i.e. T_e) versus time in the case of Ni from simulations.
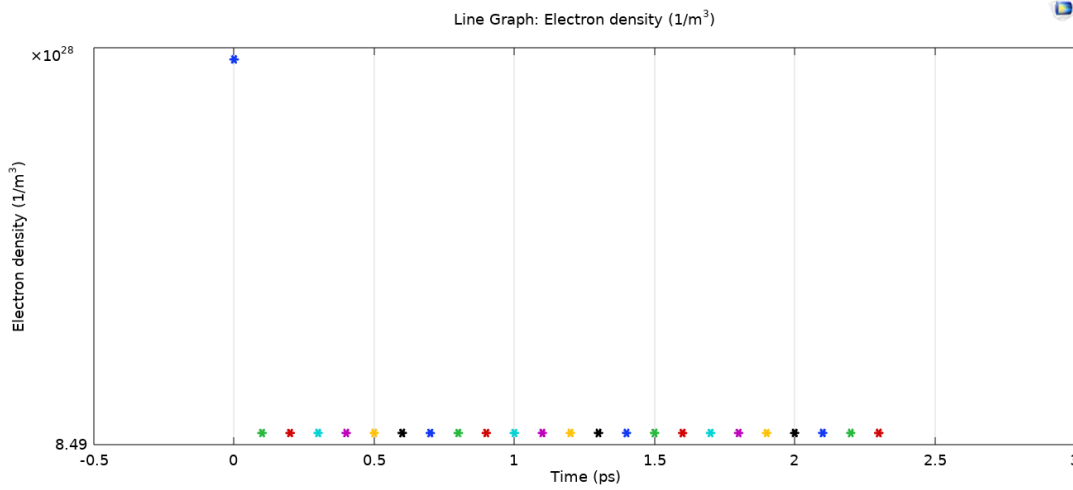

Figure 10. The plot of electron density (i.e. n_e) versus time in the case of Ni from simulations.
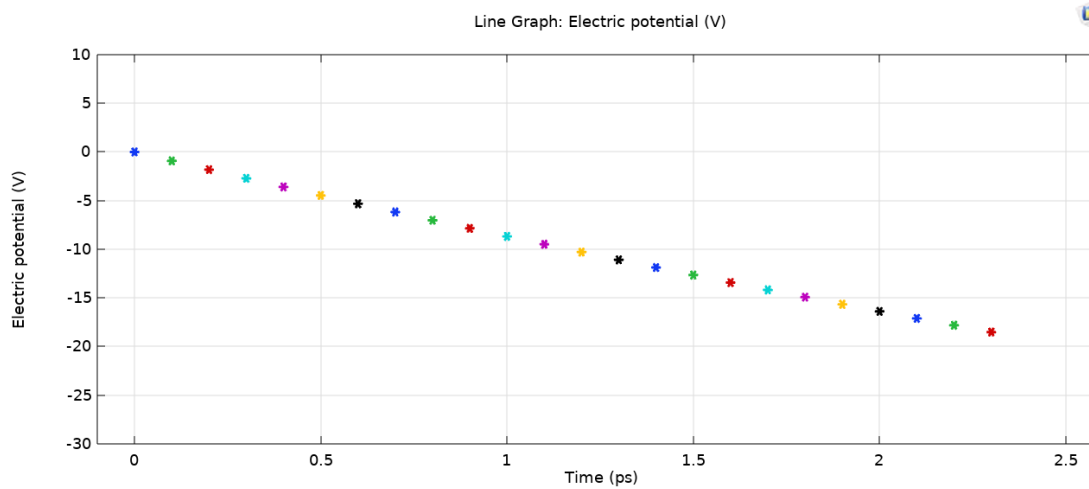

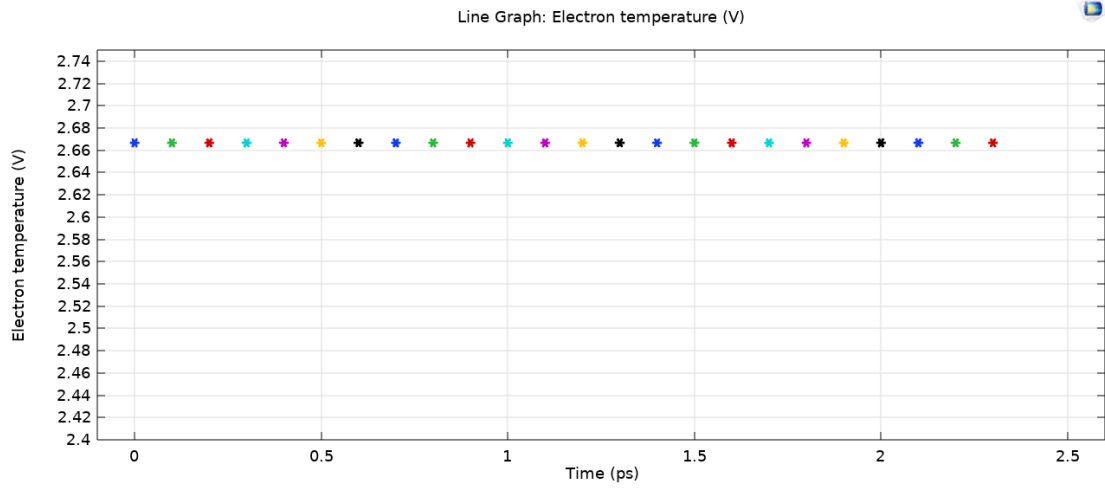*Figure 11. The plot of electric potential versus time in the case of W from simulations.*

83

Figure 12. The plot of electron temperature (i.e. T_e) versus time in the case of W from simulations.
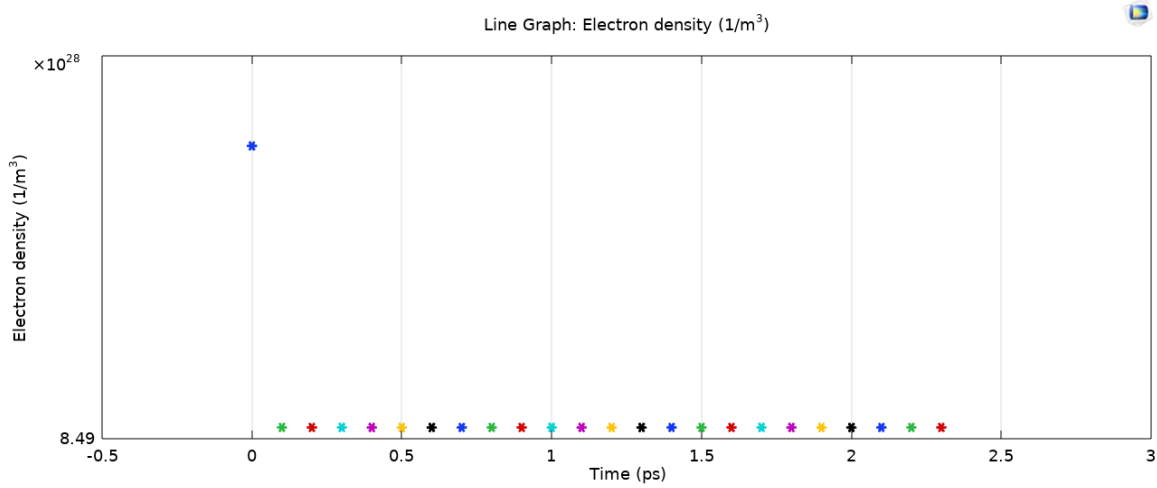

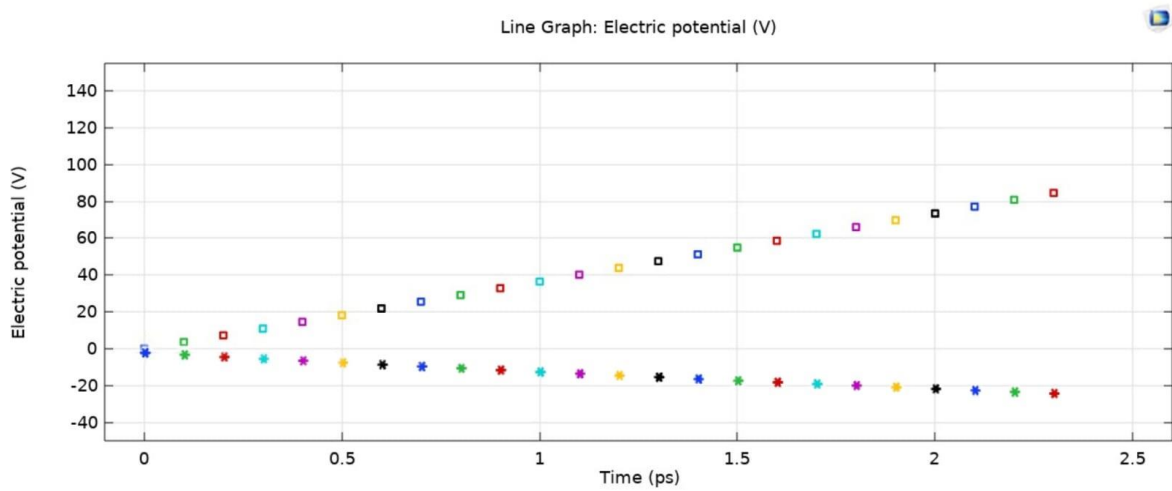*Figure 13. The plot of electron density (i.e. n_e) versus time in the case of W from simulations.*

Figure 14. The comparison of electric potential values for Ni and W.

The squares and asterisks represent the electric potentials generated for the simulations with Ni and W materials, respectively. In the W simulations, Table 3 has been employed for the laser excitation. The outcomes are displayed in Figs. 15 to 17. These results indicate that Tungsten requires a significantly higher laser power than Nickel. Notably, the analysis solely focused on a single shot laser pulse simulation to compare material and laser characteristics, there was no observation or demonstration of plasma generation, as previously mentioned.

Table 3. The features of the laser pulse used in the simulations for the W plates.

Power of The Laser	$1.5x10^{15} [W]$
Range	$2.3 [ps]$
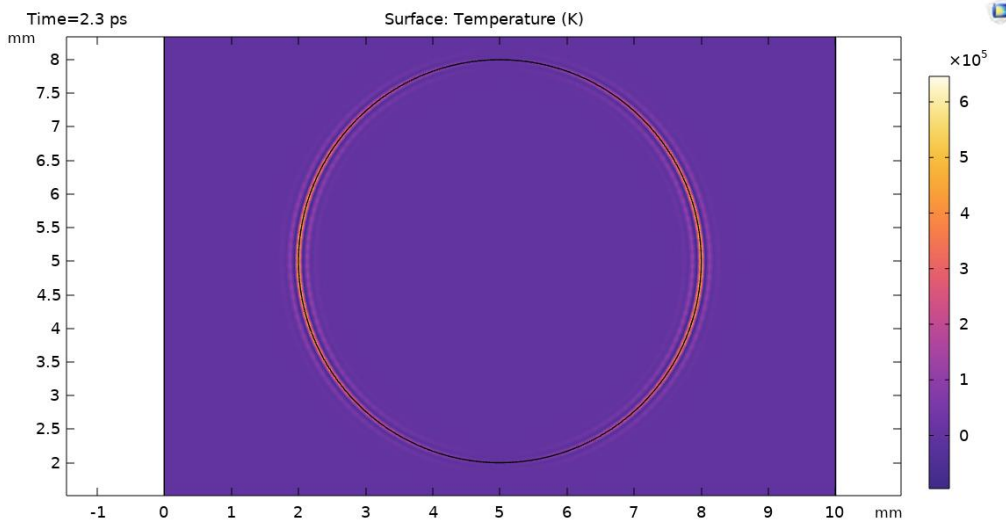
Figure 15. Illustrated laser pulse simulation with using a 2D Plate For W.
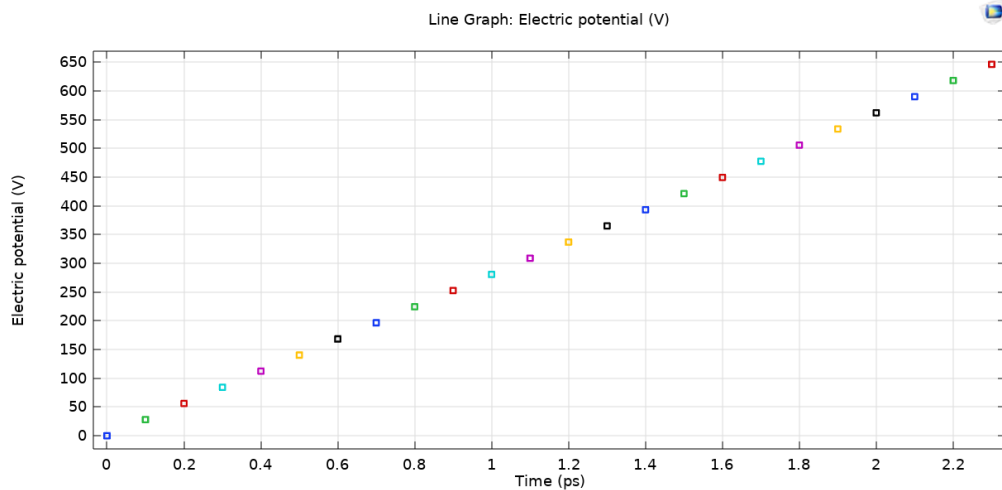
Figure 16. The plot of electric potential versus time in the case of W from simulations for higher electric potentials in the case of high-power laser.

Comparison of Figs. 11 and 16 reveals that under the conditions of the first simulation, the electric potential of Tungsten was negative, indicating the absence of electron binding and thus no current induced by electric potential. Conversely, in the second simulation, Tungsten's electric potential is

positive under the conditions given in Table 3, representing the successful electron binding and generation of current.

In the proposed laser induced capacitive inductive system design, the utilization of Tungsten as the target zone in the model offers several advantages, primarily due to its significantly lower heat of fusion, approximately half that of Nickel. Tungsten enables the application of laser pulses with considerably higher powers, thus allowing for much higher temperatures, given its melting point is over double that of Nickel. Consequently, Tungsten was designated as the target zone for the laser pulses to generate plasma. The ability to apply greater power to Tungsten may result in the generation of a quicker and denser plasma, thereby influencing the magnitude of the resultant magnetic field, potentially amplifying it further.

5. CONCLUSION

In conclusion, this article briefly introduces and discusses several methods to achieve strong magnetic field exceeding a kilotesla. It covers the generation of fields through laser-driven capacitor-coil targets and the explores various methods for field generation. The article also outlines commonly used measurement techniques and formulas for necessary calculations. The process of generating strong magnetic fields is concisely explained and required formulas for calculations are given. The nature behind the magnetic field generation in laser-driven capacitor-coil targets is briefly explained and the variations that can be made for different results are discussed, allowing room for further developments in this area. A new capacitive inductive design is featured and clarified. Magnetic field generation with this new design is observed and the results are given. According to the electromagnetic confinement methodology, such high magnetic fields cannot be reached for the nuclear fusion studies [39,40,41], whereas we believe that the laser induced capacitive inductive systems can be used for this conventional systems, too.

The characteristics of strong, enduring and controllable magnetic fields produced by laser-driven coil targets have gathered significant interest and find broad applications in high-energy density physics. This article offers a new perspective for upcoming studies in this domain. Similar to laser power's dependence on the disk material used in the generation of strong magnetic fields over 100 T, the investigation of laser frequency and coil shape may also be a subject for further research.

REFERENCES

[1] Fujioka, S., Zhang, Z., Ishihara, K., Shigemori, K., Hironaka, Y., Johzaki, T., Sunahara, A., Yamamoto, N., Nakashima, H., Watanabe, T., Shiraga, H., Nishimura, H., & Azechi, H., Kilotesla Magnetic Field due to a Capacitor-Coil Target Driven by High Power Laser, Scientific Reports, 3(1) (2013), 01170;1-7, DOI: 10.1038/srep01170

[2] Murdin, B., Li, J., Pang, M., Bowyer, E., Litvinenko, K., Clowes, S., et al., Si:P as a laboratory analogue for hydrogen on high magnetic field white dwarf stars, Nature Communications, 4(1) (2013), 1469;1-7, DOI: 10.1038/ncomms2466

[3] Gilch, P., Pollinger-Dammer, F., Musewald, C., Michel-Beyerle, M., Steiner, U., Magnetic Field Effect on Picosecond Electron Transfer, Science (New York, N.Y.), 281(5379) (1998), 982-984, DOI: 10.1126/science.281.5379.982

[4] Lai, D., Matter in Strong Magnetic Fields. Reviews of Modern Physics, 73 (2001), 629-661, DOI: 10.1103/RevModPhys.73.629

[5] Zhang, Z., Zhu, B., Li, Y., Jiang, W., Yuan, D., Wei, H., et al., Generation of strong magnetic fields with a laser-driven coil, High Power Laser Science and Engineering, 6 (2018), e38;1-8, DOI: 10.1017/hpl.2018.33

[6] Sano, T., Inoue, T., Nishihara, K., Critical magnetic field strength for suppression of the Richtmyer-Meshkov instability in plasmas, Physical Review Letters, 111(20) (2013), 205001;1-5, DOI: 10.1103/PhysRevLett.111.205001

[7] Matsuo, K., Nagatomo, H., Zhang, Z., Nicolaï, P., Sano, T., Sakata, S., et al., Magnetohydrodynamics of laser-produced high-energy-density plasma in a strong external magnetic field, Physical Review E, 95(5-1) (2017), 053204, DOI: 10.1103/PhysRevE.95.053204

[8] Plechaty, C., Presura,. R, Stein, S., Martinez, D., Neff, S., Ivanov, V., et al., Penetration of a laser-produced plasma across an applied magnetic field, High Energy Density Physics, 6(2) (2013), 258-261, DOI: 10.1016/j.hedp.2009.12.006

[9] Albertazzi, B., Ciardi, A., Nakatsutsumi, M., Vinci, T., Béard, J., Bonito, R., et al., Laboratory formation of a scaled protostellar jet by coaligned poloidal magnetic field, Science (New York, N.Y.), 346(6207) (2014), 325-328, DOI: 10.1126/science.1259694

[10] Schaeffer, D., Fox, W., Haberberger, D., Fiksel, G., Bhattacharjee, A., Barnak, D., et al., High-Mach number, laser-driven magnetized collisionless shocks, Physics of Plasmas, 24(12) (2017), 122702;1-11, DOI: 10.1063/1.4989562

[11] Byvank, T., Banasek, J., Potter, W., Greenly, J., Seyler, C., Kusse, B.. Applied axial magnetic field effects on laboratory plasma jets: Density hollowing, field compression, and azimuthal rotation, Phys Plasmas, 24(12) (2017), 122701;1-11, DOI: 10.1063/1.5003777

[12] Matsuo, K., Higashi, N., Iwata, N., Sakata, S., Lee, S., Johzaki, T., et al., Petapascal Pressure Driven by Fast Isochoric Heating with a Multipicosecond Intense Laser Pulse, Phys Rev Lett, 124(3) (2020), 035001;1-8 DOI: 10.1103/PhysRevLett.124.035001

[13] Tatarakis, M., Watts, I., Beg, F., et al., Measuring huge magnetic fields, Nature, 415(6869), p. 280 (2003). DOI: 10.1038/415280

[14] Wagner, U., Tatarakis, M., Gopal, A., Beg, F., Clark, E., Dangor, A.E., et al., Laboratory measurements of 0.7 GG magnetic fields generated during high-intensity laser interactions with dense plasmas, Physical Review E, 70(2) (2004), 026401;1-5, DOI: 10.1103/PhysRevE.70.026401

[15] Santos, J., Bailly-Grandvaux, M., Giuffrida, L., Forestier-Colleoni, P., Fujioka, S., Zhang, Z., et al., Laser-driven platform for generation and characterization of strong quasi-static magnetic fields, New Journal of Physics, 17 (2015), 083051;1-10 DOI: 10.1088/1367-2630/17/8/08305

[16] Fujioka, S., Zhang, Z., Ishihara, K., Shigemori, K., Hironaka, Y., Johzaki, T., et al., Kilotesla Magnetic Field due to a Capacitor-Coil Target Driven by High Power Laser, Scientific Reports, 3 (2013), 1170;1-7, DOI: 10.1038/srep01170

[17] Zhu, B., Li, Y., Yuan, D., Li, Y., Li, F., Liao, G., et al., Strong magnetic fields generated with a simple open-ended coil irradiated by high power laser pulses, Applied Physics Letters, 107(26) (2015), 261903;1-5 DOI: 10.1063/1.4939119

[18] Chang, P.Y., Fiksel, G., Hohenberger, M., Knauer, J.P., Betti, R., Marshall, F.J., et al., Fusion yield enhancement in magnetized laser-driven implosions, Phys Rev Lett, 107(3) (2011), 035006;1-4, DOI 10.1103/PhysRevLett.107.035006

[19] Pollock, B., Froula, D., Davis, P., Ross, J., Fulkerson, S., Bower, J., et al., High magnetic field generation for laser-plasma experiments, Review of Scientific Instruments, 77(11) (2016), 114703;1-6, DOI: 10.1063/1.2356854

[20] Froula, D., Ross, J., Pollock, B., Davis, P., James, A., Divol, L., et al., Quenching of the Nonlocal Electron Heat Transport by Large External Magnetic Fields in a Laser-Produced Plasma Measured with Imaging Thomson Scattering, Physical Review Letters, 98(13) (2007), 135001;1-4, DOI: 10.1103/PhysRevLett.98.135001

[21] Higginson, D.P., Revet, G., Khiar, B., Béard, J., Blecher, M., Borghesi, M., et al., Detailed characterization of laser-produced astrophysically-relevant jets formed via a poloidal magnetic nozzle, High Energy Density Physics, 23 (2017), 48-59, DOI: 10.1016/j.hedp.2017.02.003

[22] Albertazzi, B., Béard, J., Ciardi, A., Vinci, T., Albrecht, J., Billette, J., et al., Production of large volume, strongly magnetized laser-produced plasmas by use of pulsed external magnetic fields, Review of Scientific Instruments, 84(4) (2013), 043505;1-7, DOI: https://doi.org/10.1063/1.4795551

[23] Daido, H., Miki, F., Mima, K., Fujita, M., Sawai, K., Fujita, H., et al., Generation of a strong magnetic field by an intense CO_2 laser pulse, Phys Rev Lett, 56(8) (1986), 846-849, DOI: 10.1103/PhysRevLett.56.846

[24] Williams, G., Patankar, S., Mariscal, D., Bude, J., Carr, C., Goyon, C., et al., Laser intensity scaling of the magnetic field from a laser-driven coil target, Journal of Applied Physics,.127(8) (2020), 083302;1-18, DOI: 10.1063/1.511716

[25] Goyon, C., Pollock, B.B., Turnbull, D.P., Hazi, A., Divol, L., Farmer, W.A., et al., Ultrafast probing of magnetic field growth inside a laser-driven solenoid, Phys Rev E, 95(3) (2017), 033208;1-12, DOI: 10.1103/PhysRevE.95.033208

[26] Chien. A., Gao, L., Zhang, S., Ji, H., Blackman, E., Chen, H., et al., Pulse width dependence of magnetic field generation using laser-powered capacitor coils, Physics of Plasmas, 28 (2021), 052105;1-10, DOI: 10.1063/5.0044048

[27] Morita, H., Pollock, B.B., Goyon, C.S., Williams, G.J., Law, K.F.F., Fujioka, S., et al., Dynamics of laser-generated magnetic fields using long laser pulses, Phys Rev E, 103(3-1) (2021), 033201, DOI: 10.1103/PhysRevE.103.033201

[28] Zhu, B., Li, Y., Yuan, D., Li, Y., Li, F., Liao, G., et al., Strong magnetic fields generated with a simple open-ended coil irradiated by high power laser pulses, Applied Physics Letters, 107(26) (2015), 261903;1-5 DOI: 10.1063/1.4939119

[29] Zhu, B., Zhang, Z., Jiang, W., Wang, J., Zhu, C., Tan, J., et al., Ultrafast pulsed magnetic fields generated by a femtosecond laser, Applied Physics Letters, 113(7) (2018), 072405;1-4, DOI: 10.1063/1.5038047

[30] Gao, L., Ji, H., Fiksel, G., Fox, W., Evans, M., Alfonso, N., Ultrafast proton radiography of the magnetic fields generated by a laser-driven coil current, Physics of Plasmas, 23(4) (2016), 043106;1-7. DOI: 10.1063/1.4945643

[31] Bailly-Grandvaux, M., Santos, J., Poye, A., Quasi-stationary magnetic fields generation with a laser-driven capacitor-coil assembly, Physical Review E, 96 (2017), 023202;1-10, DOI: 10.1103/PhysRevE.96.023202

[32] Chubar, O., Elleaume, P., Chavanne, J., A three-dimensional magnetostatics computer code for insertion devices, J. Synchrotron Radiation, 5 (1998), 481-484, DOI: 10.1107/S0909049597013502

[33] Morita, H., Fujioka, S., Generation, measurement, and modeling of strong magnetic fields generated by laser-driven micro coils., Reviews of Modern Plasma Physics, 7:13;1-45 (2023), DOI: 10.1007/s41614-023-00115-6

[34] Liao, G.-Q., Li, Y., Zhu, B.-J., Li, Y., Li, F., Mengchao, Li., et al., Proton radiography of magnetic fields generated with an open-ended coil driven by high power laser pulses, Matter and Radiation at Extremes, 1(2016), 187-191, DOI: 10.1016/j.mre.2016.06.003

[35] Strickland, D., Mourou, G., Compression of amplified chirped optical pulse, Optics Communications, 56(3) (1985), 219-221, DOI: 10.1016/0030-4018(85)90120-8

[36] Li, X.X., Cheng, R.J., Wang, Q., Liu, D.J., Lv, S.Y., Huang, Z.M., et al, Anomalous staged hot-electron acceleration by two-plasmon decay instability in magnetized plasmas, Phys Rev E.,108(5) (2023), L053201;1-6. DOI: 10.1103/PhysRevE.108.L053201

[37] Peebles, J.L., Davies, J.R., Barnak, D.H., Garcia-Rubio, F., Heuer, P.V., Brent, G., et al., An assessment of generating quasi-static magnetic fields using laser-driven "capacitor" coils, Phys Plasmas, 29(8) (2022), 080501;1-28, DOI: 10.1063/5.0096784

[38] Dursun, B., Kurt, E., Tekerek, M., A power circuit design for the poloidal field coils in a torus-shaped plasma system, JES, 2019;3(3):123-128. DOI: 10.30521/jes.609667

[39] Kurt, E., Dursun, B. Particle Trajectories and Energy Distribution from a New IEC Fusion Device: A Many-Body Approach., J. Fusion Energy 35, 483–492 (2016). DOI: 10.1007/s10894-015-0033-2

[40] Dursun, B., Kurt, E., Kurt, H., Energy distributions and radiation emissions in an inertial electrostatic confinement (IEC) device under low and moderate magnetic fields, Int. J. Hydrogen Energy, 42 (2017), 17874-17885, DOI: 10.1016/j.ijhydene.2017.02.015